Article

Protective Coatings for Ferritic Stainless Steel Interconnect Materials in High Temperature Solid Oxide Electrolyser Atmospheres

Jyrki Mikkola [1,*], Karine Couturier [2], Belma Talic [3,†], Stefano Frangini [4], Nathalie Giacometti [2], Nathalie Pelissier [2], Bhaskar Reddy Sudireddy [3] and Olivier Thomann [1,‡]

1. Fuel Cells and Hydrogen Team, VTT Technical Research Centre of Finland Ltd., P.O. Box 1000, 02044 Espoo, Finland; olivier.thomann@neste.com
2. CEA (Atomic Energy and Alternative Energies Commission)-LITEN (Innovative Laboratory for New Energies Technologies and Nanomaterials), Université Grenoble Alpes, 38054 Grenoble, France; karine.couturier@cea.fr (K.C.); nathalie.giacometti@cea.fr (N.G.); nathalie.pelissier@cea.fr (N.P.)
3. Department of Energy Conversion and Storage, Technical University of Denmark, Anker Engelunds Vej 301, 2800 Kongens Lyngby, Denmark; belma.talic@sintef.no (B.T.); bhsu@dtu.dk (B.R.S.)
4. ENEA (Energia Nucleare ed Energie Alternative), CR (Casaccia Centro Ricerche), TERIN-PSU-ABI, 00123 Rome, Italy; stefano.frangini@enea.it
* Correspondence: jyrki.mikkola@vtt.fi
† Current address: SINTEF Industry, Sustainable Energy Technology, P.O. Box 124, Blindern, 0314 Oslo, Norway.
‡ Current address: Neste Oyj, Innovation, Discovery and External Collaboration, P.O. Box 310, 06101 Porvoo, Finland.

Abstract: Stainless steel interconnect materials used in solid oxide fuel cells and electrolysers need to be coated to improve oxidation resistance and to mitigate Cr-vaporization. This work aimed to explore the optimal steel/coating combinations suitable for use in reversible solid oxide stacks and evaluated $(Co,Mn)_3O_4$ spinel, $LaFeO_3$ perovskite, Ce/Co and Y-based coatings, on AISI441 and Crofer 22 APU steels. The coatings were evaluated based on measurements of mass gain and oxide scale thickness after exposure at 700 and 800 °C to fuel side (90 vol.% H_2O/10 vol.% H_2) and air/oxygen side (pure O_2) atmospheres. In pure O_2, the most efficient coatings for limiting oxide scale formation and Cr evaporation, compared to the bare steel, were $(Co,Mn)_3O_4$ and CeCo on Crofer 22 APU. In 90 vol.% H_2O/10 vol.% H_2, the Y-based coating showed the largest improvement in oxidation resistance.

Keywords: fuel cells; solid oxide cells; interconnects; degradation; protective coatings

1. Introduction

The use of renewable energy has gained increasing interest in recent years as the importance of the reduction in greenhouse gas emissions has been recognized. In the ongoing transition of the electricity market, spatiotemporal variations in energy demand and supply are increasing as renewable, variable energy sources, mainly wind and solar power, are becoming more common [1].

Solid oxide cell (SOC) technology offers a viable option for the long-term storage of energy [2]. A reversible solid oxide cell (rSOC) system can operate in electrolysis mode, to produce H_2 and O_2 from gaseous H_2O, and in fuel cell mode, to convert the stored H_2 to electricity. Moreover, SOCs can be used for co-electrolysis of water and carbon dioxide to produce syngas, which can be further processed into synthetic fuels [3]. The high operating temperature of SOC (typically 600–850 °C) enables a higher efficiency in comparison to other existing fuel cell and electrolysis technologies [4]. However, challenges with high material costs and degradation issues related to the high operation temperature hinder a more widespread commercial adaptation of SOC technology [5].

The interconnect plates are a critical component, and their durability affects the overall lifetime of the stack. The interconnects plates are used in stacks to separate fuel and oxidant, to connect the cells electrically in series, and to give mechanical support for the stack. To fulfill these functions, the optimal interconnect material for SOCs should have a low electrical resistivity, high thermal conductivity, and a coefficient of thermal expansion (CTE) matching with the other stack components [5,6]. It should also be chemically stable in both oxygen and fuel electrode atmospheres at high temperatures. Ferritic stainless steels meet many of these criteria and are therefore commonly used as interconnect material. Specially tailored steel grades with a high chromium content for enhanced oxidation resistance have been designed [7]. Nonetheless, there are several challenges with ferritic stainless steel interconnects that negatively impact the lifetime and performance of SOCs.

During the operation of the SOCs, oxidation of the ferritic stainless steel interconnect plates leads to the formation of a protective Cr_2O_3 scale that increases the electrical resistivity and thus lowers the efficiency of the fuel cell stack and system. Additionally, chromium evaporated from the interconnect surface as chromium oxyhydroxide $CrO_2(OH)_2$ and chromium oxide (CrO_3) can deposit onto the oxygen electrode material and degrade its electrochemical activity and thereby the performance of the cell, stack, and system [6,8].

Although these issues have been extensively studied for solid oxide fuel cell (SOFC) mode of operation, less work has been undertaken to investigate the durability of interconnects in solid oxide electrolyser (SOEC) mode of operation, where the conditions to which the interconnects are exposed are somewhat different. As oxygen is produced during SOEC operation, there may be a higher partial pressure of oxygen on the air/oxygen side of the interconnect compared to SOFC operation. However, this depends on system design and how the produced oxygen is handled. In some solutions, high air purge is used, making the difference between SOFC and SOEC minimal. In other cases, a purge gas might not be used in order to valorize the produced oxygen, in which case the interconnect will be exposed to pure oxygen. Studies on how the oxygen partial pressure influences the corrosion rate of ferritic stainless steels have so far produced contradictory results. Palcut et al. [9] found that the oxidation rates were clearly higher when annealed in pure oxygen compared to air, whereas Alnegren et al. [10] reported that the oxidation rates were essentially independent of the oxygen partial pressure. There may be several explanations for this discrepancy, such as the use of different gas flow rates, different levels of humidification, or differences in the pre-treatment of the steel samples. Clearly, more research is needed to clarify the effect of the oxygen partial pressure.

On the fuel side, the difference between the two modes of operation is that in SOEC mode, the H_2O/H_2 ratio decreases from the inlet to the outlet, whereas, in SOFC mode, it is the opposite. Young et al. [11] showed that H_2O (up to 20 vol.%) has a detrimental effect on the fuel side corrosion rate, especially at lower temperature. The H_2O content in the fuel side of rSOC may be as high as 90 vol.%, but there is very little research on how such a high H_2O content affects the degradation of the steel.

Regardless of the operating mode, protective coatings are needed to protect steel interconnect plates from oxidation and the oxygen electrodes from chromium poisoning. Different interconnect steel compositions and different coatings and deposition methods have been extensively investigated for SOFC operation [12,13].

For the oxygen side, $(Co,Mn)_3O_4$ spinel coatings have been shown to be good candidates with various deposition methods and compositional variations having been tested [14–29]. Ce/Co coatings, deposited as a metallic layer and oxidized to a spinel during operation in the stack, have also showed promising chromium retention and oxidation protection properties [30–35]. Most of these oxidation studies have been in air (targeting SOFC mode of operation), but Molin et al. [36] studied a Co_3O_4 spinel-based coating in oxygen-rich atmospheres at temperatures between 800 and 900 °C and reported promising properties.

Interesting results have been recently obtained also with chemical LaFeO3 (LFO) perovskite coatings produced by molten salt surface modification treatments [37–39]. These

treatments have been carried out at around 600 °C in La_2O_3-containing molten carbonate reaction baths. The interconnect steel reacts with the La_2O_3 reactant dissolved in the melt to form a dual perovskite-spinel oxide structure comprising a mixed Fe-Cr oxide as the inner layer and $LaFeO_3$ as the outer layer. Cr presence in the outer perovskite layer is minimized because Cr dissolves in the reaction bath as soluble chromate during the iron conversion process, which represents a further advantage. Perovskite LFO coatings with variable structures and thicknesses ranging from the sub-micron level to several microns can be obtained by properly tuning reaction conditions and bath chemical composition [37]. Functional properties and oxidation resistance, including the influence of coating thickness, were studied thoroughly on K41 and Crofer 22H steel grades under SOFC conditions, namely at 700 °C in humid air (3% relative humidity). The poorly aerated molten salt reaction medium causes the formation of an oxygen defective oxide structure, which undergoes a rapid mass gain during the initial stages of a high temperature air exposure. The best electrical contact properties and minimal initial mass gain were observed with thinner coatings layers produced under accelerated reaction conditions by adding CuO or nitrate accelerants to the reaction medium.

For the fuel side, few works have been published to date, and not necessarily with the coatings studied in the present work. The positive effect of Ce and La coatings on the oxidation rate of an interconnect steel in $Ar/5$ vol.% $H_2/3$ vol.% H_2O atmosphere has been demonstrated at 850 °C [40]. LSM and Co_3O_4 coatings have been demonstrated to limit the oxide scale growth and maintain a low ASR after 3000 h at 800 °C in $Ar/1$ vol.% $H_2/9$ vol.% H_2O [41]. However, the decomposition of LSM to La_2O_3 and MnO in fuel side atmosphere makes it disputable whether this coating will act as an efficient protective layer in the SOEC environment. No studies have been so far conducted on LFO coating stability in rSOC fuel side environments but thermogravimetric studies report that $LaFeO_3$ is stable at 1000 °C in a wide O_2 partial pressure range and that it decomposes to La_2O_3 and metallic Fe only at partial pressure of O_2 below 10–16.95 bar [42]. This suggests that $LaFeO_3$ should be stable under the typical reducing side SOC conditions. However, the dual spinel-perovskite nature may pose some doubts about the effective stability of the LFO coatings due to the presence of highly reducible mixed Fe-Cr spinel oxides underneath the perovskite layer. Finally, a thin yttrium-based coating has been shown to provide effective protection against corrosion of Crofer 22 APU steel at 750 °C in 90 vol.%/10 vol.% steam-hydrogen atmosphere [43].

In this study, $(Co,Mn)_3O_4$ spinel, $LaFeO_3$ perovskite, Ce/Co, and Y-based coatings, which have shown promising properties in both SOFC and SOEC atmospheres, were studied at 700 and 800 °C in both fuel side and oxygen side atmospheres. The coatings were tested on AISI 441 steel, which is a low-cost commercial ferritic stainless steel, and on Crofer 22 APU, which is a more expensive, specially designed steel grade. The objective of the work was to determine the optimal steel/coating combinations to be used as interconnect materials in reversible solid oxide stacks.

2. Materials and Methods

2.1. Materials

For oxidation tests, two steel grades with and without coatings were studied in both O_2 and H_2O-H_2 atmospheres representing the O_2-enriched air and fuel sides in SOEC operation, respectively. The steel alloys Crofer 22 APU (EN. 1.4760) and AISI 441 (EN. 1.4509) in plates of 0.2 mm thickness were chosen as the interconnect substrate. AISI 441 steel is a low-cost commercial ferritic stainless steel grade, used in various applications, that contains ~18 wt.% chromium. Crofer 22 APU is a more expensive, specially designed steel grade, developed for solid oxide fuel cell applications, that contains ~22 wt.% chromium. The elemental compositions of both steels are specified in Table 1.

Table 1. Composition of the steels used as interconnect substrates.

wt.%	Cr	C	Si	Mn	P	S	Ti	Nb	Cu	La	Fe
Crofer 22 APU [44]	20–24	0.03	0.5	0.3–0.8	0.05	0.02	0.03–0.2	-	0.5	0.04–0.2	Bal.
AISI 441 [45]	17.5–18.5	$\leq$0.03	$\leq$1	$\leq$1	$\leq$0.04	$\leq$0.015	0.1–0.6	$(3 \times C + 0.30) - 1$	-	-	Bal.

The steels were tested both in the "as-received" condition and coated. In total, two coatings on the H_2O-H_2 side and three coatings on the O_2 side were evaluated. For the H_2O-H_2 atmosphere, uncoated, lanthanum ferrite (LFO) coated and Y-coated steels were tested. For the O_2 side tests, $Co_{1.5}Mn_{1.5}O_4$ (MCO), LFO and Ce/Co coated steels were studied in addition to uncoated steels.

Coating Preparation

Before deposition of the $Co_{1.5}Mn_{1.5}O_4$ and Y-coatings the steel substrates were cleaned ultrasonically for 10 min in acetone and 10 min in ethanol. Before deposition of the LFO coating, the substrates were cleaned for 10 min in acetone.

The $Co_{1.5}Mn_{1.5}O_4$ spinel coating with a thickness of about 20 µm was prepared by electrophoretic deposition (EPD) at DTU, similar to the way reported by Bobruk et al. [46]. The suspension for EPD was made by mixing ethanol and isopropanol (50:50 by volume) with iodine (0.2 wt.% of solvents) and adding the $Co_{1.5}Mn_{1.5}O_4$ powder (2 wt.% of solvents, American Elements). The suspension was ball milled for two days before use. The set-up for EPD consisted of a Teflon box (ca. 150 mL) with two steel counter electrodes mounted in parallel in order to deposit on both sides of the sample. The steel coupon to be coated was mounted in parallel between the counter electrodes and immersed in the coating solution. The deposition was carried out at 60 V for 60 s. The coated sample was subsequently sintered in two steps (red-ox sintering): first at 1000 °C for 2 h in N_2-9 vol.% H_2 and thereafter at 800 °C for 5 h in air.

The Y-coating with a thickness less than 0.3 µm was prepared by electrolytic deposition (ELD) at DTU. The solution for ELD was prepared by dissolving 0.05 M $Y(NO_3)_3$ in ethanol. The same set-up as described for EPD was used for ELD, but the deposition was in this case carried out at 40 V for 60 s. After deposition, the coated samples were rinsed with ethanol, dried with compressed air, and heat treated on a hot plate (ca. 400 °C) for 1 min to convert the coating from a Y-hydroxide to Y_2O_3. A more detailed description of the coating procedure can be found in Ref. [43].

The La-Fe perovskite was applied by a chemical conversion coating process in a molten carbonate bath in a 20 h process at 600 °C under CO_2 gas bubbling at ENEA. The molten carbonate chemical bath contained Li_2CO_3, Na_2CO_3, La_2O_3 and MgO, in addition to CuO, added to accelerate the reaction and to reduce coating thickness. Due to its scarce molten carbonate solubility, the accelerating effect of CuO is due to galvanic Fe/Cu coupling between the dispersed CuO particles in the molten salt and steel surface, which means that the galvanic coupling action is strongly dependent on particle size. For these experiments, LFO formation was accelerated using a CuO particle size of ca. 10 µm. Although these reaction conditions were not optimized for a maximum coating thickness reduction, nonetheless they were sufficient to reduce thickness by one-half as compared to non-accelerated coatings (see [38]). During the process, Fe in the steel component forms solid protective product layers with the molten carbonate bath, whereas Cr dissolves in the molten carbonate bath. A Cr-contaminated salt layer often remains adherent on the coating surface after the treatment. This layer was removed by soaking the coated steel samples in acetone followed by prolonged cleaning in boiling deionized water. The final coating structure was composed of a $LaFeO_3$ polycrystalline perovskite layer (about 3–8 µm thickness) also containing some sporadically dispersed Cu metallic particles. The spinel sublayer consisted of a relatively thick (8–12 µm) structure, which was separated into two distinct layers consisting of a Fe-rich oxide layer above a mixed Fe-Cr oxide layer.

Finally, the Ce/Co coating was prepared by Sandvik Materials Technology AB using physical vapor deposition (PVD). The Co layer was 600 nm thick and the Ce layer beneath was 10 nm thick. The metallic layers are oxidized rapidly during first hours of exposure at high temperature (>700 °C) in an oxidizing atmosphere, and therefore the coating is in practice composed mainly of CeO_2 and Co_3O_4 based on the work of J.-E. Svensson's team [15,30,47]. The AISI 441 samples were coated with a Sandvik's roll-to-roll mass production coating line, whereas the Crofer 22 APU samples were coated in a batch based PVD process.

2.2. Oxidation Tests

Oxidation tests were conducted at two different temperatures, 700 and 800 °C. With Crofer 22 APU, tests were performed at 700 and 800 °C in O_2 and H_2O-H_2 atmospheres. With AISI 441, tests were carried out in O_2 atmosphere at 700 and 800 °C and in an H_2O-H_2 atmosphere at 800 °C.

For each steel/coating combination, two to five parallel samples were tested. All samples, coated and uncoated, were cleaned before oxidation tests. First, samples were kept for 10 min in an ultrasonic bath in acetone and then for another 10 min in an ultrasonic bath in ethanol. Finally, they were dried at room temperature with compressed air.

The testing parameters are presented in Table 2. Tests were performed in three laboratories at VTT, DTU and CEA, using the same temperature and atmosphere, but slightly different gas velocities. The gas linear velocities calculated for the different reactor diameter and gas flows used at different partners laboratories are presented in Table 3. For all exposures, the samples were heated at 1 °C/min to the exposure temperature at which they were kept for a total of 1500 h. After 150, 300, 450, 600, 900 and 1500 h of aging at the exposure temperature, the furnace was cooled and each sample weighed before re-heating and continuation of the test. The sample weights were measured on a scale with 0.01 mg resolution. A heating rate of 1 °C/min was used in all transitions. In O_2 atmosphere, heating, aging, and cooling were all carried out in pure O_2. In H_2O-H_2 atmosphere, heating up and cooling down were performed in N_2-5 vol.%H_2 and at the exposure temperature, H_2 and O_2 were mixed to produce 90 vol.%H_2O-10 vol.%H_2. For safety reasons, the O_2 was introduced 10 s after introducing pure H_2.

Table 2. Parameters for oxidation tests.

Temperature Ramps	Heating Up and Cooling Down Atmospheres	Exposure Temperatures	Exposure Atmospheres	Exposure Time
1 °C/min	Oxidizing atmosphere: Pure O_2 Reducing atmosphere: N_2/5 vol.% H_2	700 °C 800 °C	Oxidizing atmosphere: Pure O_2 Reducing atmosphere: 90 vol.% H_2O/10 vol.% H_2	1500 h

Table 3. Gas linear velocities used in the tests.

Steel	Atmosphere	Temperature (°C)	Partner	Gas Linear Velocity (cm/s)
Crofer 22 APU	O_2	700	VTT	0.2
Crofer 22 APU	O_2	800	VTT	0.3
Crofer 22 APU	H_2-H_2O	700	DTU	1.1
Crofer 22 APU	H_2-H_2O	800	DTU	1.3
AISI 441	O_2	700	CEA	3.5
AISI 441	O_2	800	CEA	3.9
AISI 441	H_2-H_2O	800	DTU	1.3

2.3. Post-Test Characterization

After aging, the samples were cold vacuum embedded in epoxy resin and polished to reveal the cross section. A carbon coating was sputtered on the surface to enhance the conductivity of the sample. Once prepared, the samples were analyzed in a scanning electron microscope (SEM) equipped with an energy dispersive X-ray spectrometer (EDS). All imaging and analysis were conducted at an acceleration voltage between 15 and 20 kV. From the SEM/EDS analysis, the microstructure, composition, and thickness of the oxide scales and coatings were analyzed.

3. Results and Discussion

3.1. Weight Gain

3.1.1. O_2 Atmosphere

The weight gains of the samples during aging in O_2 at 700 and 800 °C are presented in Figure 1. Weight gains are presented as averages with standard deviations, except for LFO coated AISI 441 at both temperatures and for LFO coated Crofer 22 APU at 800 °C, for which the weight gains are plotted separately for the two samples tested due to the large difference in mass gain.
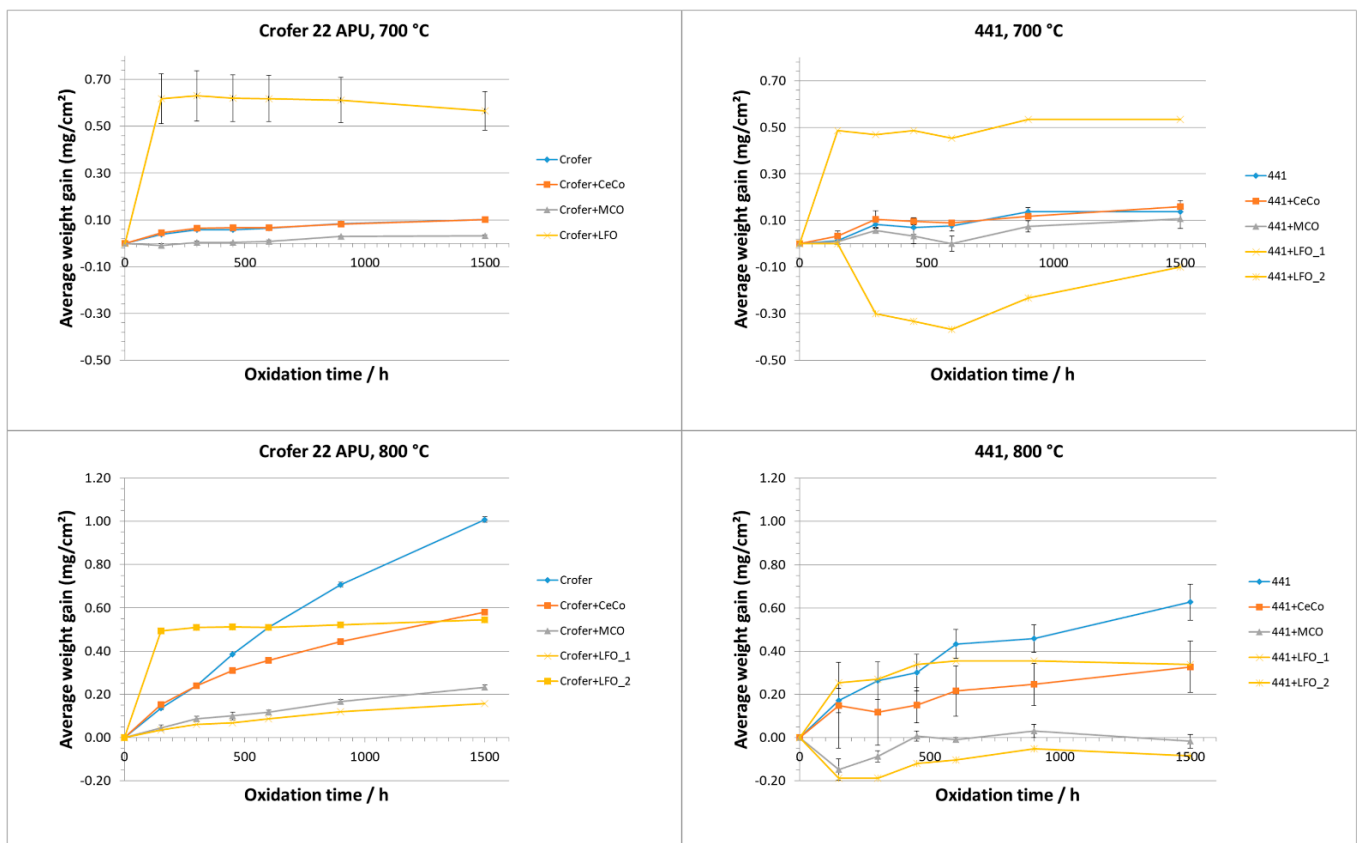

Figure 1. Average weight gain of the samples in oxidizing atmosphere at 700 °C (**upper row**) and 800 °C (**lower row**) with standard deviations. For the Ce/Co coated samples, 0.19 mg/cm^2 is subtracted from the initial weight gain to account for oxidation of Co.

The Ce/Co coated samples showed a large weight gain during the first 150 h of oxidation, on average 0.30 ± 0.14 mg/cm^2 for both AISI 441 and Crofer 22 APU samples at both temperatures. Part of this weight gain can be explained by the fact that the originally metallic Ce/Co coating itself was oxidized during the first hours of exposure to high temperature, as shown previously by Froitzheim et al. [15]. Assuming complete oxidation of the 600 nm thick metallic Co coating to Co_3O_4 corresponds to a weight gain of 0.19 mg/cm^2.

This value was subtracted from the weight gain data of the Ce/Co coated samples presented in Figure 1. Thus, the weight gains presented in Figure 1 represent almost entirely the weight gain due to oxidation of the steel.

LFO coated samples clearly showed the largest weight gain on both steels at 700 °C. At 800 °C, spallation of the coating was observed after completion of the oxidation test (1500 h), as can be seen in Figure 2. There is a strong possibility that spallation also occurred earlier during the test and, thus, the weight gain data for LFO coated samples is not trustworthy at 800 °C. The mass loss behavior of some LFO coated samples at 700 °C indicates that spallation may also be a problem at this temperature, even though it was not visually observed after the test.
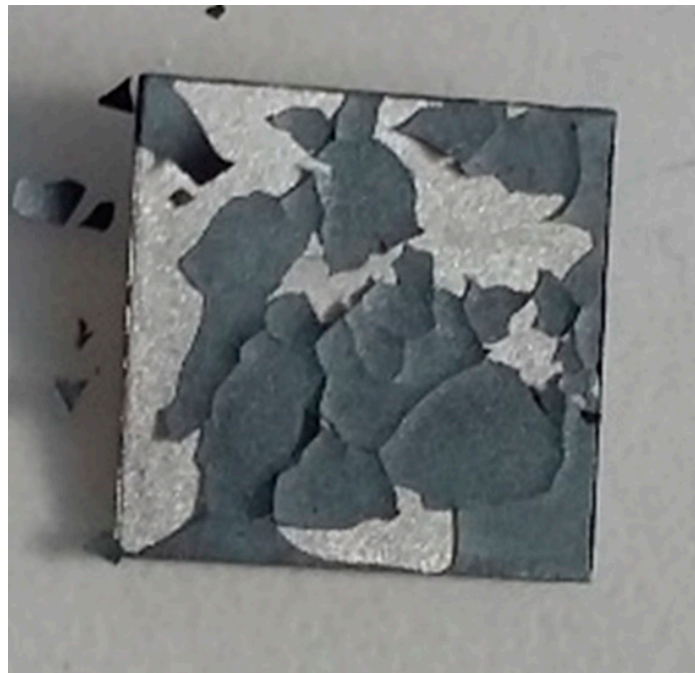

Figure 2. LFO coated AISI 441 after 1500 h aging in O_2 at 800 °C.

Visual inspection after the 1500 h oxidation test did not show any sign of spallation or Fe-oxide formation on the surface of uncoated, MCO, and Ce/Co coated steels at either temperature, with the exception of some Ce/Co coated AISI 441 samples at 800 °C. In these samples, some signs of delamination were observed after 300 h of oxidation, which likely explains the high variation in weight gain observed among the Ce/Co coated samples. This was not observed at 700 °C or with Ce/Co coated Crofer 22 APU at either temperature. Otherwise, the weight gain behavior was similar for the Crofer 22 APU and AISI 441 samples at both temperatures. In all cases, the MCO coated samples showed the lowest absolute weight gains.

At 800 °C, the Ce/Co coated samples had clearly lower weight gain rates compared to the uncoated samples. The weight gain of Ce/Co coated samples was 0.60 mg/cm^2 for Crofer 22 APU and 0.35 mg/cm^2 for AISI 441 samples, whereas the same numbers for uncoated samples were 1.0 and 0.65 mg/cm^2, respectively. For MCO coated samples, weight gains at 800 °C were 0.25 mg/cm^2 for Crofer 22 APU and 0.0 mg/cm^2 for AISI 441.

At 700 °C, no clear difference was seen in the weight gain rate between Ce/Co coated samples and uncoated samples, whereas MCO coated samples still had the lowest weight gain values. As has been shown previously, uncoated samples have higher Cr evaporation rates than coated ones [15,29,30]. Cr evaporation causes mass loss and, thus, the weight gain caused by oxidation might actually be higher for uncoated sample than the measured mass gain.

At 800 °C, the Crofer 22 APU samples had unexpectedly higher weight gain rates than AISI 441, whereas the weight gains were more similar at 700 °C. This could be due to the fact that the O_2 gas flow velocity during the oxidation was 0.3 cm/s for Crofer 22 APU samples, whereas it was 3.9 cm/s for AISI 441 samples. The higher gas velocity can lead to a higher Cr evaporation rate, which may be the reason why AISI 441 samples had lower weight gain rates. However, the relative impact of Cr evaporation with respect to scale growth on the mass gain/loss typically increases with decreasing temperature [32], which implies that the difference between Crofer 22 APU and AISI 441 should be even bigger at 700 °C than at 800 °C. Here, the weight gain rates were more similar between steel grades at 700 °C, i.e., the opposite of what may be expected. Furthermore, it has been previously shown that Ce/Co and MCO coatings provide very good protection against Cr evaporation [14–16,30], so the difference between the Ce/Co and MCO samples at 800 °C cannot be explained based on Cr evaporation. A possible explanation for these unexpected results is that the Crofer 22 APU samples and AISI 441 samples were tested in different laboratories with different furnaces, so it is possible that there may have been minor differences in the temperature and gas humidity during the oxidation.

Based on the results at 700 and 800 °C on Crofer 22 APU and AISI 441, it appears that the MCO spinel deposited by EPD is an efficient coating for limiting steel oxidation in an oxidizing atmosphere.

3.1.2. H_2-H_2O Atmosphere

Oxidation resistance testing in H_2-H_2O was performed in an atmosphere containing 90 vol.% of H_2O and 10 vol.% of H_2 representing a high steam content at the SOEC fuel electrode inlet or the SOFC outlet when operated with a high fuel utilization. Weight gain data are shown in Figure 3. LFO coated samples already showed severe spallation after 150 h at 700 °C, as can be seen in Figure 4. The samples were not oxidized further and, because of the poor performance at 700 °C, it was decided to exclude this steel/coating combination from the test at 800 °C.
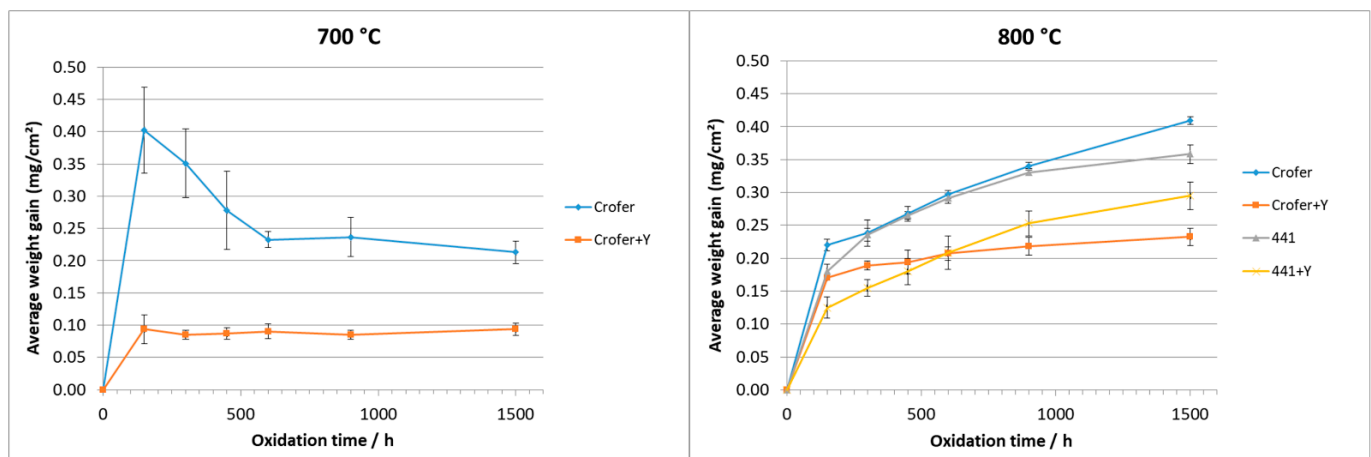

Figure 3. Average weight gain of the samples in reducing atmosphere at 700 °C and 800 °C with standard deviations.
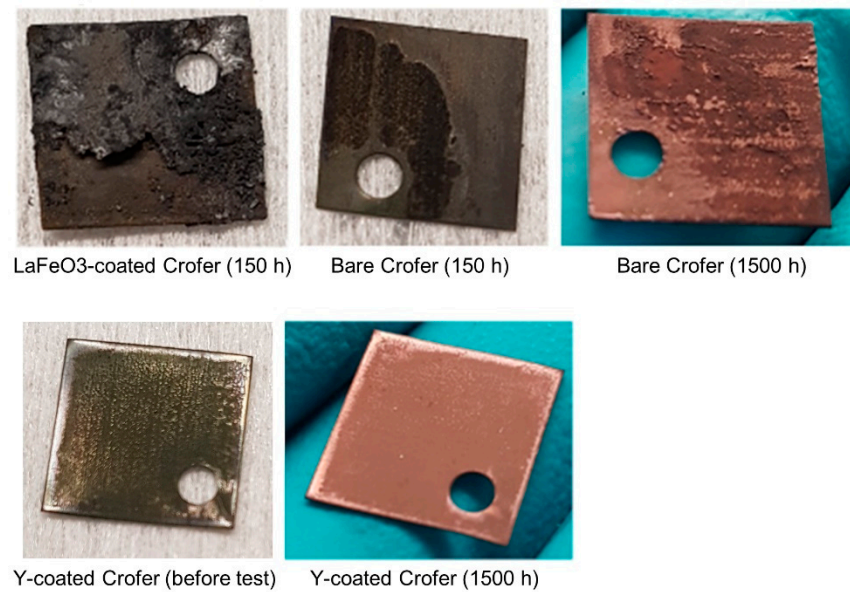
Figure 4. Pictures of the samples after aging in H_2-H_2O atmosphere at 700 °C.

A high mass gain was recorded for uncoated Crofer 22 APU after 150 h of aging at 700 °C and visual inspection of the samples showed signs of oxide scale spallation (see Figure 4). This signals that uncoated Crofer 22 APU already undergoes break-away oxidation in the first 150 h of aging. With further oxidation, the mass decreased continuously, which can be attributed to further spallation of the oxide scale. From visual inspection at the end of the oxidation test (1500 h, Figure 4), the surface of the uncoated Crofer 22 APU samples appeared with severe spallation and a reddish hue, indicating Fe-oxide formation and break-away oxidation. The Y-coated samples showed promising behavior at 700 °C as there was only a small weight increase during the first 150 h and apparently no weight change with further oxidation. Visual inspection of the Y-coated samples after 1500 h of aging showed no sign of spallation (Figure 4). The edges of this sample appeared shinier than the center, possibly due to a difference in the thickness of the Y coating.

In contrast to the observations at 700 °C, the uncoated Crofer 22 APU showed no signs of spallation over the entire duration of the oxidation test at 800 °C (see Figure 1). Nevertheless, the Y-coated sample showed again more promising properties than the uncoated steel. At 800 °C, the total average weight gain for Y-coated Crofer 22 APU samples after 1500 h of aging was 0.25 mg/cm^2, whereas it was 0.40 mg/cm^2 for uncoated samples, as shown in Figure 5.
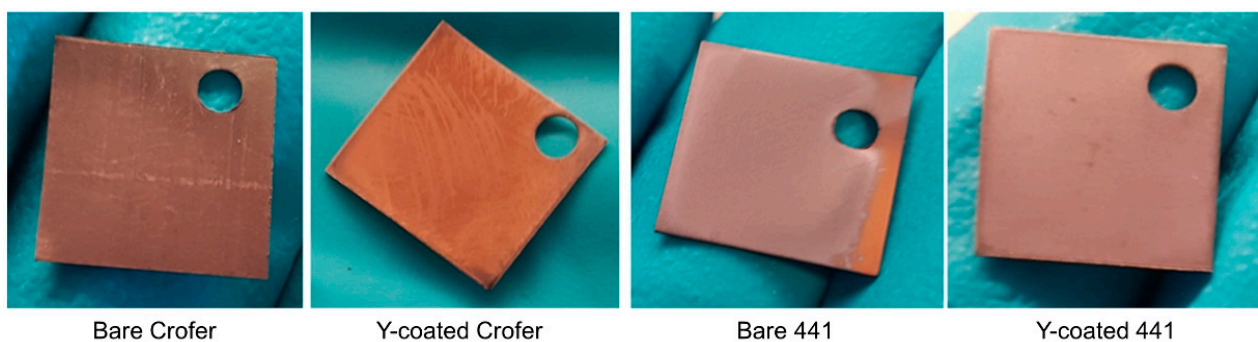

Figure 5. Pictures of the samples after aging in H_2-H_2O atmosphere at 800 °C.

The uncoated AISI 441 samples showed similar weight gain values as the uncoated Crofer 22 APU. The Y-coating reduced the weight gain relative to the uncoated steel, but the reduction was relatively lower in the case of AISI 441 than in the case of Crofer 22 APU. Regarding Crofer 22 APU at 800 °C, no severe spallation was observed with visual inspection. However, one of the uncoated AISI 441 samples showed signs of iron oxide formation on parts of the sample surface (reddish hue, right-hand side of sample shown in Figure 1).

Based on the data at 700 and 800 °C, it may be concluded that the Y-coating deposited by ELD is an efficient coating for reducing the oxidation of both Crofer 22 APU and AISI 441 in the fuel side atmosphere. For the uncoated Crofer 22 APU, it is clear that exposure to 700 °C represents harsher conditions than exposure to 800 °C.

3.2. Post-Test Analysis

3.2.1. O_2 Atmosphere

After oxidation in pure oxygen at both temperatures, a chromium oxide layer was formed on top of both uncoated steels. Above this oxide scale, there was an additional oxide layer that includes manganese and chromium. This layer was identified as a $(Cr,Mn)_3O_4$ spinel oxide, which usually has higher electrical conductivity than chromia. Moreover, internal oxidization was observed, especially in AISI 441 steel, but also in the Crofer 22 APU in the first microns beneath the steel surface. This can be seen as dark spots near the surface of the steels in Figure 6. The internal oxides were confirmed to be TiO_2 and SiO_2 particles via EDS analysis. These observations are in line with previous studies of Crofer 22 APU and AISI 441 oxidized in pure oxygen at the temperature range of 600–950 °C [10,48,49].

The MCO coated samples had a homogeneous oxide layer, comprised of chromium oxide (possibly with some Mn, Co, and Fe), between the steel and the coating material, as can be seen in Figure 7. There was only a minor amount of chromium detected in the coating layer—1.5 at.% with Crofer 22 APU and 0.2 at.% with AISI 441—as shown in Figure 8 and Table 4. This small difference in Cr content is explained by the fact that EDS analysis from the coating layer was undertaken further away from the steel-coating interface with AISI 441 than with Crofer 22 APU, as can be seen in Figure 8. Moreover, amount of iron in the coating layer was minimal in both cases. Thus, there was no clear presence of iron or chromium in the MCO coating layer, which indicates that the coating was efficient in limiting cation diffusion and Cr evaporation outward from the steel, as has been previously reported [26,28,50]. The adhesion of the coating was good on the Crofer 22 APU samples. In the AISI 441 samples, there was a gap between the steel and the oxide layer in part of the sample, which was most probably formed during the SEM sample preparation (see Figure 8). Nevertheless, this may indicate that the AISI 441 steel has poorer adhesion to the oxide scale than Crofer 22 APU. Oxide scale detachment was also seen with the Ce/Co samples and with all the AISI 441 samples tested in reducing atmosphere, as shown later in this article. Weak adhesion properties in AISI 441 steel have been previously reported in the literature. Chandra-Ambhorn et al. [51] explain that the oxidation of silicon to silica at the steel/scale interface facilitates crack propagation and scale spallation. Moreover, the high molybdenum content in AISI 441 causes intermetallic precipitates at the metal/scale interface and chromia scales have poor adhesion to these intermetallic phases that have very low chromium amount. Moreover, the absence of rare earth metals in AISI 441 has been suggested as the possible reason for the lower scale adhesion in AISI 441 [50–52].
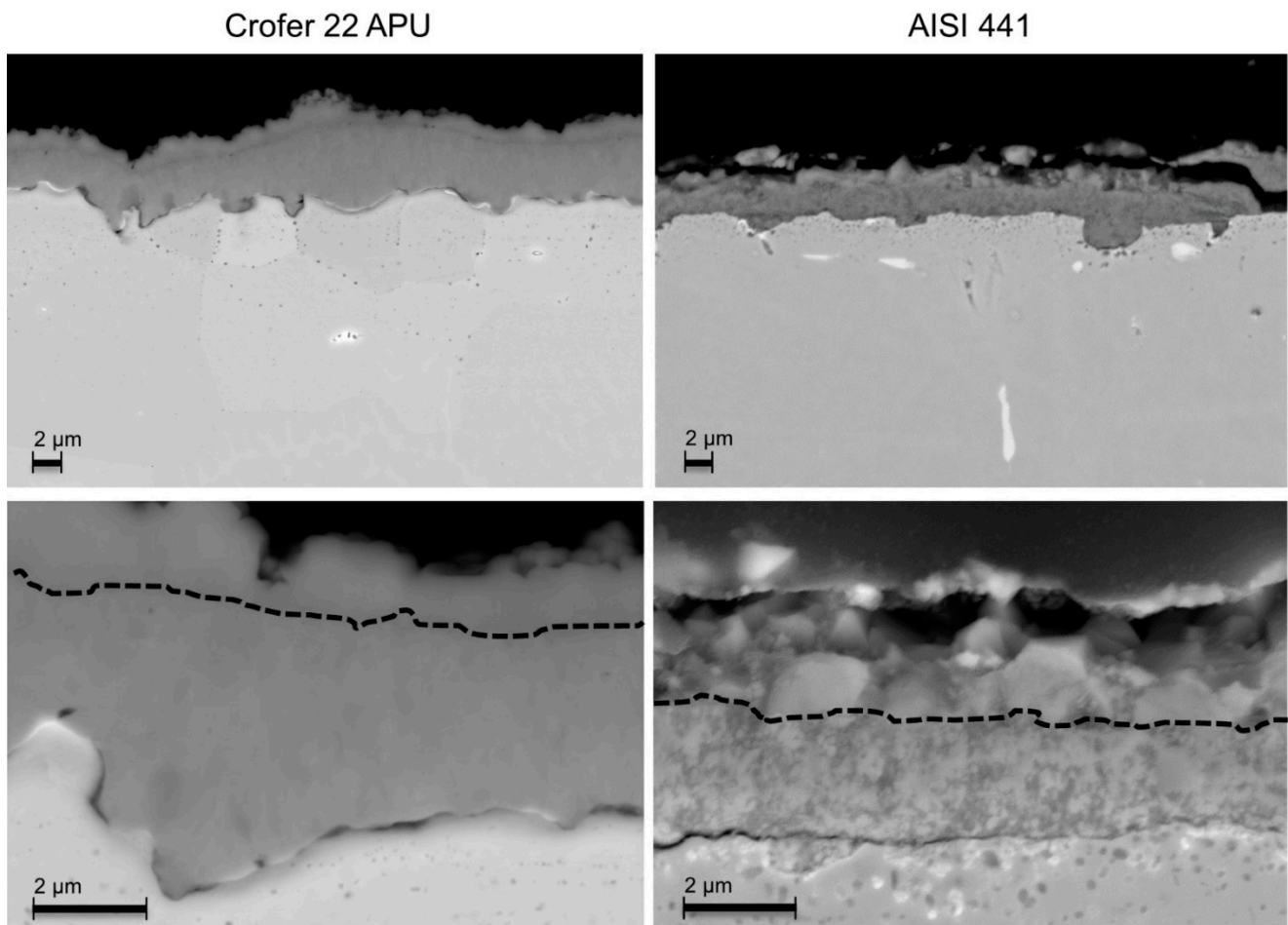
Figure 6. Uncoated Crofer 22 APU (**left**) and AISI 441 (**right**) after 1500 h at 800 °C in oxidizing atmosphere, showing 2500× (**upper**) and 10,000× (**lower**) magnifications. Dashed black lines show approximately the interface between chromia and $(Cr,Mn)_3O_4$ spinel oxides in the pictures at higher magnification.

Table 4. Element concentrations in wt./at.% measured with EDS analysis of MCO coated Crofer 22 APU and AISI 441 after 1500 h at 700 °C. The location of the analysis spots is marked in Figure 8. The presence of Al likely originates from the polishing process.

Spot	O wt./at.%	Al wt./at.%	Si wt./at.%	Cr wt./at.%	Mn wt./at.%	Fe wt./at.%	Co wt./at.%
1—Crofer 22 APU	29.9/60.1	0.6/0.7	0.2/0.2	2.4/1.5	23.2/13.6	-	43.8/23.9
2—Crofer 22 APU	32.2/61.7	0.5/0.6	0.2/0.2	30.2/17.8	8.8/4.9	4.6/2.5	23.4/12.2
3—Crofer 22 APU	-	0.5/1.1	0.1/0.2	23.1/24.3	-	76.2/74.5	-
1—AISI 441	25.4/54.8	0.2/0.3	0.4/0.5	0.3/0.2	23.7/14.9	1.2/0.7	48.5/28.4
2—AISI 441	28.3/57.4	0.1/0.2 (Ti 1/0.7)	0.2/0.3	29.8/18.7	9.9/5.8	3.6/2.1	26.7/14.7
3—AISI 441	-	(Ti 0.5/0.4)	0.7/1.4	18.1/19.2	0.3/0.3	79.6/78.6	(Nb 0.7/0.5)

Crofer 22 APU

AISI 441
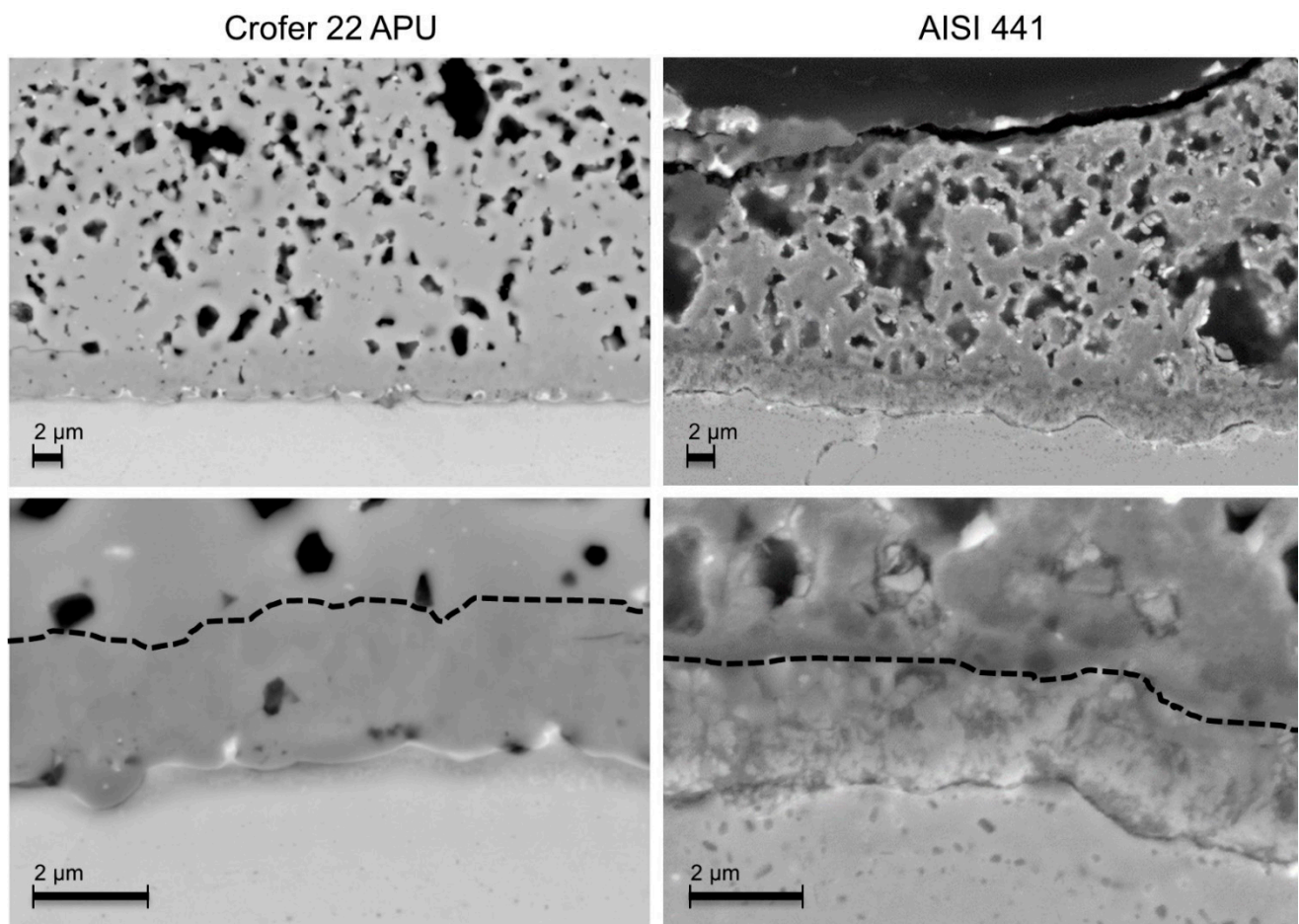
2 µm

2 µm

2 µm

2 µm

Figure 7. MCO coated Crofer 22 APU (**left**) and AISI 441 (**right**) after 1500 h at 800 °C in oxidizing atmosphere at 2500× (**upper**) and 10,000× (**lower**) magnifications. Dashed black lines approximately show the interface between the oxide scale and the MCO coating in the pictures at higher magnification.
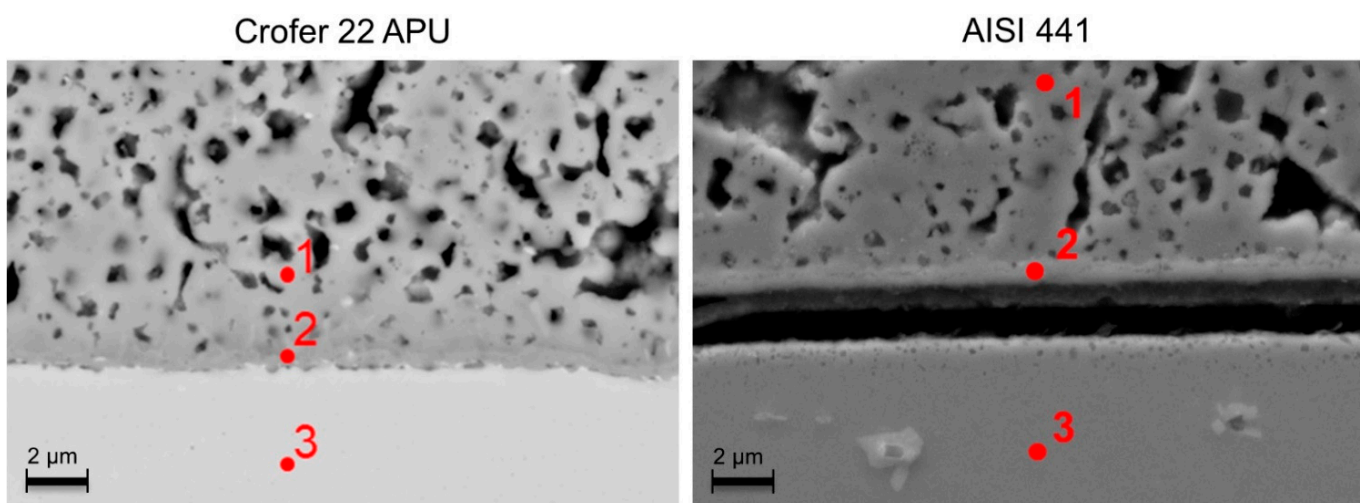
Crofer 22 APU

AISI 441

2 µm

2 µm

Figure 8. MCO coated Crofer 22 APU (**left**) and AISI 441 (**right**) after 1500 h at 700 °C. EDS point analysis was conducted from three spots indicated by red markers. The compositions in these spots are given in Table 4.

The Ce/Co coated Crofer 22 APU and AISI 441 samples oxidized at 700 °C had a homogenous oxide layer structure with an inner (Cr,Co,Mn,Fe)-oxide layer which can be divided into Mn-containing chromia and (Co,Mn,Fe)-oxide for AISI 441 (see EDS maps in Figure 9), and an outer cobalt oxide layer. Between these layers, there was a thin ceria layer, which can be seen as bright particles in the SEM pictures in Figure 9. At 800 °C, the oxide layers between the Crofer 22 APU steel and ceria layer consisted of an inner Cr_2O_3 layer and an outer Cr,Mn,Co-spinel layer. The outermost coating layer is cobalt manganese oxide, in which only a minimal amount (<5 wt.%) of iron detected. For AISI 441 samples at 800 °C, inner Cr_2O_3 and (Cr,Mn)-spinel oxides were also characterized but neither Co nor Ce was detected by EDS. This indicated that the outer Co oxide and ceria layer probably delaminated after the 1500h oxidation test. This observation could be correlated with the presence of pores detected in Co oxide, and between the chromia and Co oxide layers, as reported by Grolig et al. [34] with the same steel and different oxidizing conditions, but to an excessive extent in this work compared to the situation in their work. The layer compositions analyzed with EDS are presented in Table 5 with the measurement points marked in Figure 9 EDS maps for Ce/Co coated AISI 441 at 700 °C are also presented in the same figure. The diffusion of manganese to the cobalt oxide coating has been reported before [31,33,47] and is beneficial for the electrical properties of the coating. Moreover, with more manganese, the coefficient of thermal expansion of the spinel is closer to that of ferritic stainless steels [19,53], which should improve the adhesion of the coating during the thermal cycling.

There was only a very slight diffusion of iron or chromium in the upper coating layer both at 700 and 800 °C (<5 wt.% of each element), which indicates that the Ce/Co coating was efficient in limiting cation diffusion and Cr evaporation outward from the steels, as has been reported in the literature [30,33,34].

LFO coated Crofer 22 APU and AISI 441 samples oxidized at 700 °C had a lanthanum ferrite layer clearly visible on the surface (seen as a bright layer in Figure 10). Beneath it there was a thick iron oxide layer that also included Cr and Cu and a thin chromium iron oxide layer. There was a ~7 wt.% maximum of chromium present in the thick iron oxide layer and no significant amount of chromium (max. 2.5 wt.%) was seen in the outmost lanthanum ferrite layer. This suggests that, at 700 °C, the LFO coating works as an effective barrier against chromium evaporation. However, after oxidation at 800 °C, there was much less lanthanum ferrite left in the coating than at 700 °C, in particular for AISI 441. The total thickness of the oxide layers was very heterogeneous after treatment at 800 °C (about 5 to 15 μm). These findings further confirm the observation that there was spallation in the LFO coated samples during or after the oxidation at 800 °C. Moreover, after oxidation at 800 °C, significant amounts of chromium were present in all the layers, in particularly for Crofer 22 APU, as shown in Figure 10 and Table 6.
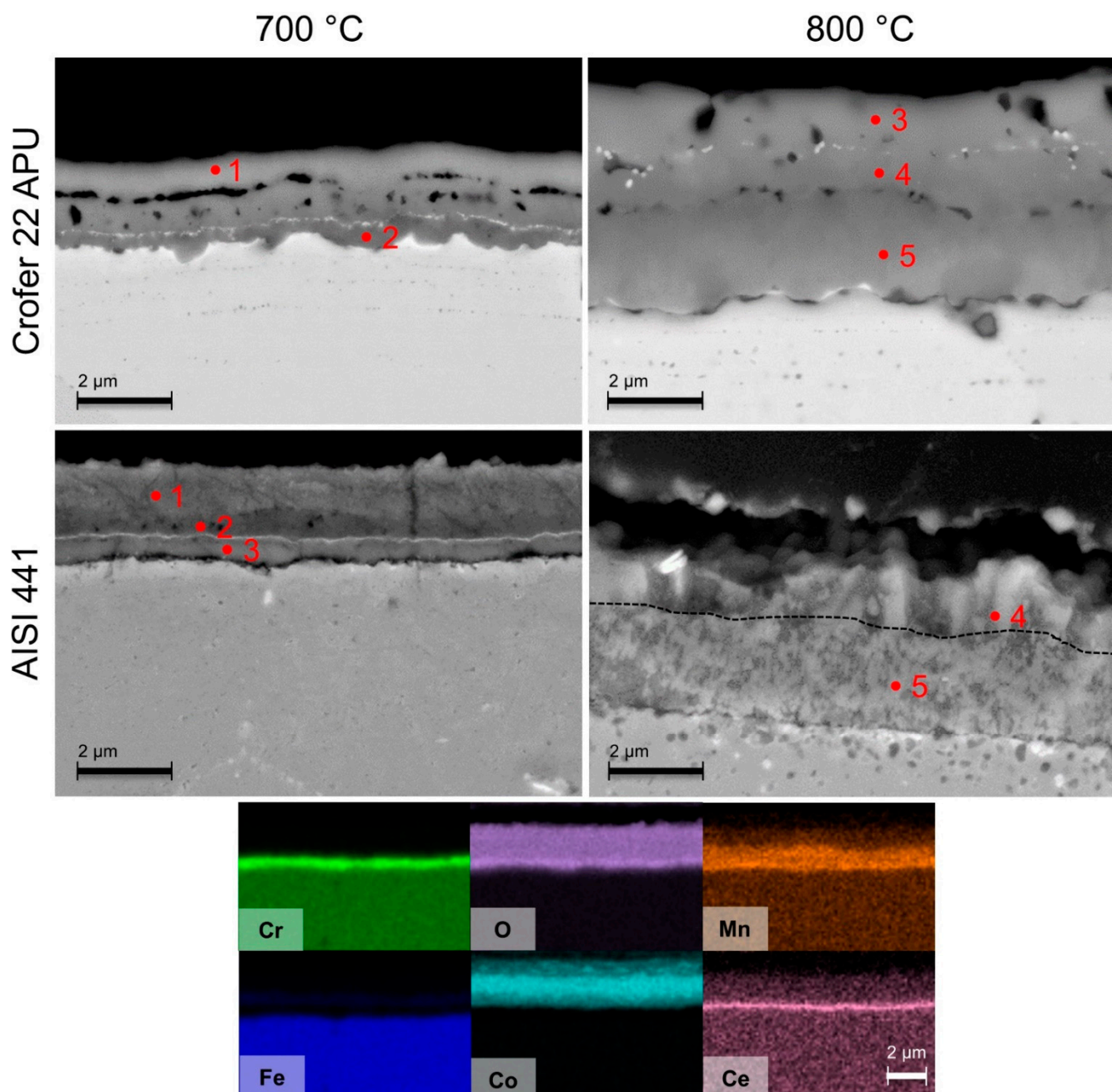
Figure 9. Ce/Co coated Crofer 22 APU (**upper**) and AISI 441 (**lower**) after 1500 h at 700 °C (**left**) and at 800 °C (**right**) in oxidizing atmosphere. The dashed line approximately shows the interface between the Cr_2O_3 oxide scale and the (Cr,Mn)-spinel oxide on the picture at 800 °C for AISI 441 (bottom right). EDS point analysis was conducted from the spots indicated by red markers. The compositions in these spots are given in Table 5. The EDS maps on the bottom are for Ce/Co coated AISI 441 at 700 °C.

Table 5. Element concentrations in wt./at.% measured with EDS analysis from Ce/Co coated Crofer 22 APU and AISI 441 after 1500 h at 700 and 800 °C. The locations of the spots are marked in Figure 9. The presence of Al likely originates from the polishing process.

Spot	O wt./at.%	Al wt./at.%	Si wt./at.%	Cr wt./at.%	Mn wt./at.%	Fe wt./at.%	Co wt./at.%
700 °C							
1—Crofer 22 APU	37.0/67.7	0.8/0.9	0.1/0.1	1.5/0.8	6.8/3.6	3.1/1.6	50.6/25.2
2—Crofer 22 APU	28.3/58.4	0.6/0.8	0.1/0.1	17.1/10.9	5.8/3.5	9.5/5.6	35.6/20.0
1—AISI 441	26.2/56.1	0.2/0.3	0.5/0.6	1.3/0.9	3.2/2.0	7.4/4.5	61.2/35.6
2—AISI 441	25.0/54.3	0.1/0.1	0.2/0.3	4.4/2.9	6.7/4.2	17.9/11.2	45.1/26.6
3—AISI 441	25.6/52.9	0.1/0.2	1.1/1.2 (Ti 2.5/1.7)	52.5/33.4	1.5/0.9	9.6/5.7	6.5/3.7
800 °C							
3—Crofer 22 APU	35.4/65.8	0.7/0.8	-	4.7/2.7	21.1/11.5	-	37.9/19.2
4—Crofer 22 APU	35.7/65.8	0.6/0.6	0.1/0.1	14.9/8.5	16.0/8.6	-	32.6/16.3
5—Crofer 22 APU	38.4/66.9	0.4/0.4	-	58.3/31.2	-	2.6/1.3	0.3/0.1
4—AISI 441	34.0/63.0	-	-	43.9/25.1	19.9/10.7	1.2/0.6	-
5—AISI 441	33.9/62.5	-	0.2/0.2	60.5/34.4	1.1/0.6	3.6/1.9	-

Based on the SEM pictures, an average thickness of the thermally grown oxide scale was determined for each steel/coating combination tested in oxidizing atmosphere (see Figure 11). These measurements confirmed the positive effect of both MCO and Ce/Co coatings compared to the uncoated steels. Smaller average values for oxide scale thicknesses were found with MCO and Ce/Co coated samples, in particular when tested at 800 °C. Due to a lower precision of measurement with the submicronic thicknesses achieved at 700 °C, the analysis is less clear at this temperature.

3.2.2. H_2-H_2O Atmosphere

SEM analysis confirmed the formation of Fe oxide on the uncoated Crofer 22 APU tested at 700 °C, which was already seen by visual inspection. The top-most porous layer in Figure 12 was confirmed to be Fe,Cr-oxide by EDS analysis. Such iron-rich oxides were not formed with the Y-coated Crofer 22 APU (see Figure 13). Instead, the oxide layer above the Y-coating consisted of manganese and chromium rich oxide with only a minimal amount of iron detected (<5 wt.%), whereas chromia was observed below the Y-coating. The Y-coating itself was deposited as a hydroxide and was converted to Y_2O_3 during the first heat treatment of the coating phase. During long-term oxidation, the coating reacts with the Cr from the steel/oxide scale to form $YCrO_3$, as shown by Molin et al. [43].

Interestingly, there was only a minimal amount of iron detected (<5 wt.%) in the oxide layers on the uncoated Crofer 22 APU after 1500 h at 800 °C in reducing atmosphere (see Figure 13). Instead, the oxide layer consisted of a thin inner Cr_2O_3 layer and a thicker $(Mn,Cr)_3O_4$ layer. The interface between the two oxide layers is characterized by pores. The same relationship between the temperature and oxidation properties and formation of protective oxide scales with ferritic stainless steels in H_2-H_2O atmosphere was previously shown by Young et al. [11]. They showed that at low temperatures of 500–550 °C, ferritic stainless steels do not form protective oxides scales when reacted with H_2-H_2O, but when the temperature increases to 650–700 °C protective chromia scales start to form. With still higher temperatures of 800–900 °C, the rate of chromia scale formation increases. These findings are aligned with the observations in this work that lower temperatures appear to be "more aggressive" in H_2-H_2O atmosphere.
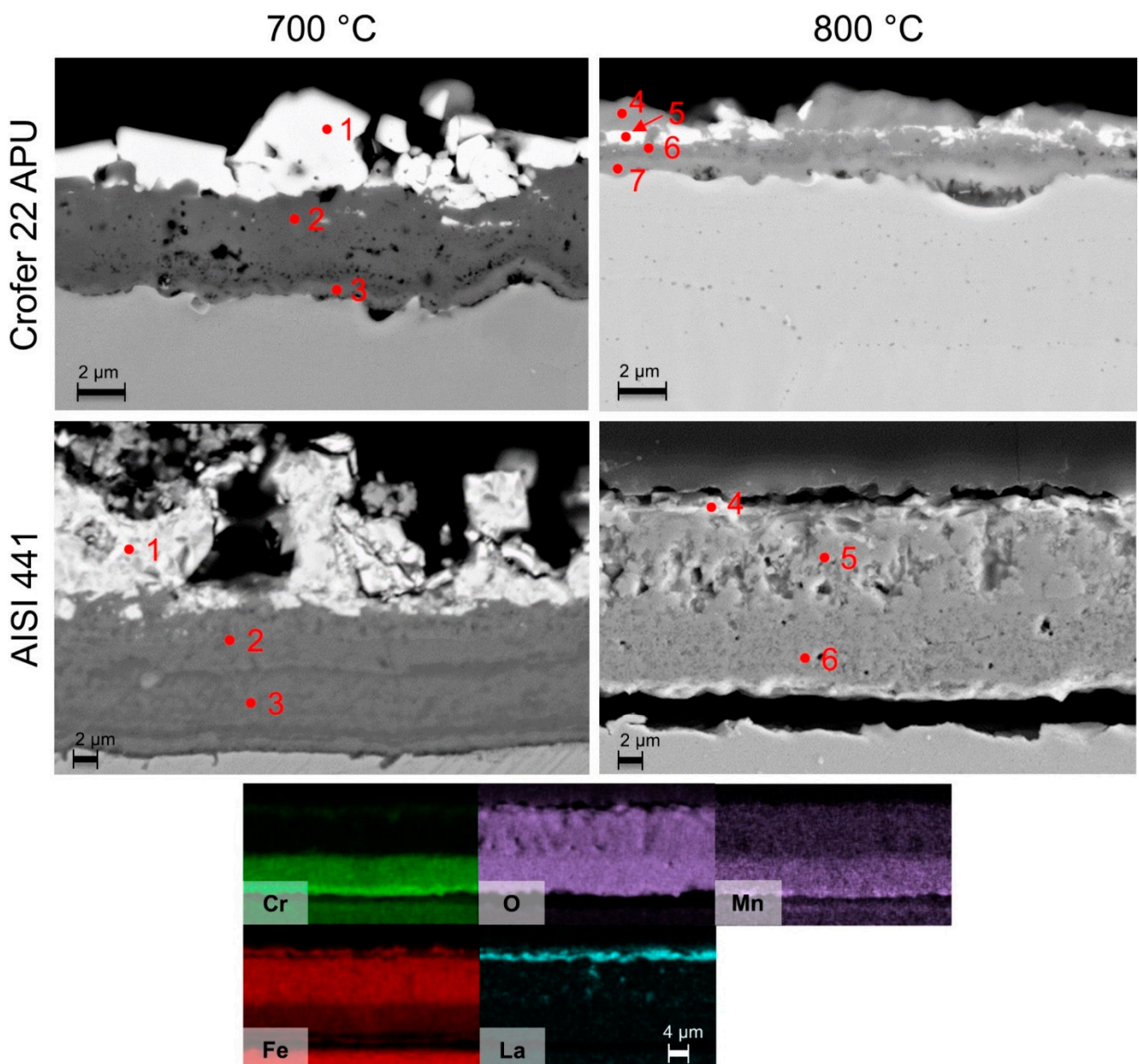
Figure 10. LFO coated Crofer 22 APU (**top**, ×5000) and AISI 441 (**bottom**, ×2500) after 1500 h at 700 °C (**left**) and at 800 °C (**right**) in oxidizing atmosphere. EDS point analysis was conducted from the spots indicated by red markers. The compositions in these spots are given in Table 6. For AISI 441 at 800 °C, EDS maps were also recorded as shown in this figure.

Table 6. Element concentrations in wt./at.% measured with EDS analysis from LFO coated Crofer 22 APU and AISI 441 after 1500 h at 700 °C and 800 °C. The location of the spots is marked in Figure 10.

| Spot	O wt./at.%	Al wt./at.%	Cr wt./at.%	Mn wt./at.%	Fe wt./at.%	Cu wt./at.%	La wt./at.%
700 °C							
1—Crofer 22 APU	18.7/56.3	0.6/1.0	0.4/0.3	-	28.4/24.4	-	51.9/17.9
2—Crofer 22 APU	29.4/59.0	0.3/0.4	7.2/4.5	3.7/2.1	53.0/30.4	5.8/2.9	-
3—Crofer 22 APU	1.7/5.6	0.3/0.6	22.3/22.5	-	75.5/71.1	-	-
1—AISI 441	19.4/54.2	1.0/1.7	2.5/2.2	(Si 1.1/1.7)	23.0/18.4	9.9/7.0	42.8/13.8
2—AISI 441	25.8/58.0	0.3/0.4	2.4/1.6	(Si 0.8/1.1)	48.9/31.5	3.5/2.0	17.9/4.6
3—AISI 441	29.9/58.7	(Si 1.3/1.5)	32.6/19.6	2.1/1.1	33.1/18.5	-	0.7/0.2
800 °C							
4—Crofer 22 APU	36.0/66.2	0.3/0.3	8.3/4.7	21.2/11.3	30.0/15.8	-	3.4/0.7
5—Crofer 22 APU	31.0/65.8	0.5/0.6	7.6/5.0	10.7/6.6	22.3/13.6	-	26.5/6.5
6—Crofer 22 APU	34.3/63.9	0.2/0.2	30.6/17.5	17.0/9.2	13.2/7.1	0.3/0.2	3.2/0.7
7—Crofer 22 APU	35.4/64.3	0.3/0.3	46.9/26.2	2.9/1.5	13.7/7.1	-	-
4—AISI 441	30.9/61.1	0.2/0.3	1.5/0.9	2.8/1.6	62.0/35.1	1.6/0.8	1.0/0.2
5—AISI 441	28.3/58.1	(Si 0.2/0.3)	3.7/2.3	2.2/1.3	63.1/37.1	1.1/0.5	1.0/0.2
6—AISI 441	29.9/58.3	0.1/0.2	43.3/26.0	3.0/1.7	21.1/11.8	1.2/0.6	(Si 1.2/1.3)
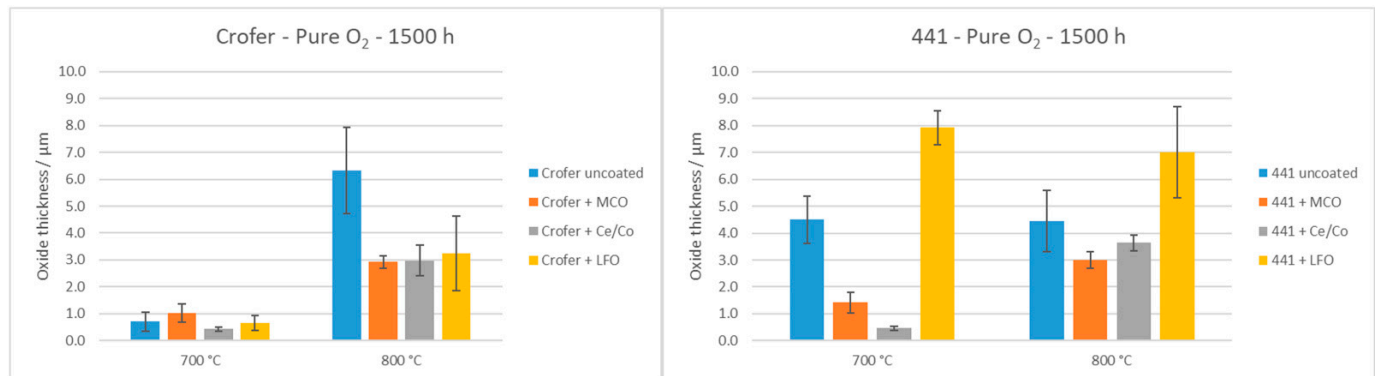
Figure 11. Average oxide scale thicknesses (including chromium-rich oxides) for Crofer 22 APU (**left**) and AISI 441 (**right**) samples tested in oxidizing atmosphere with standard deviations.
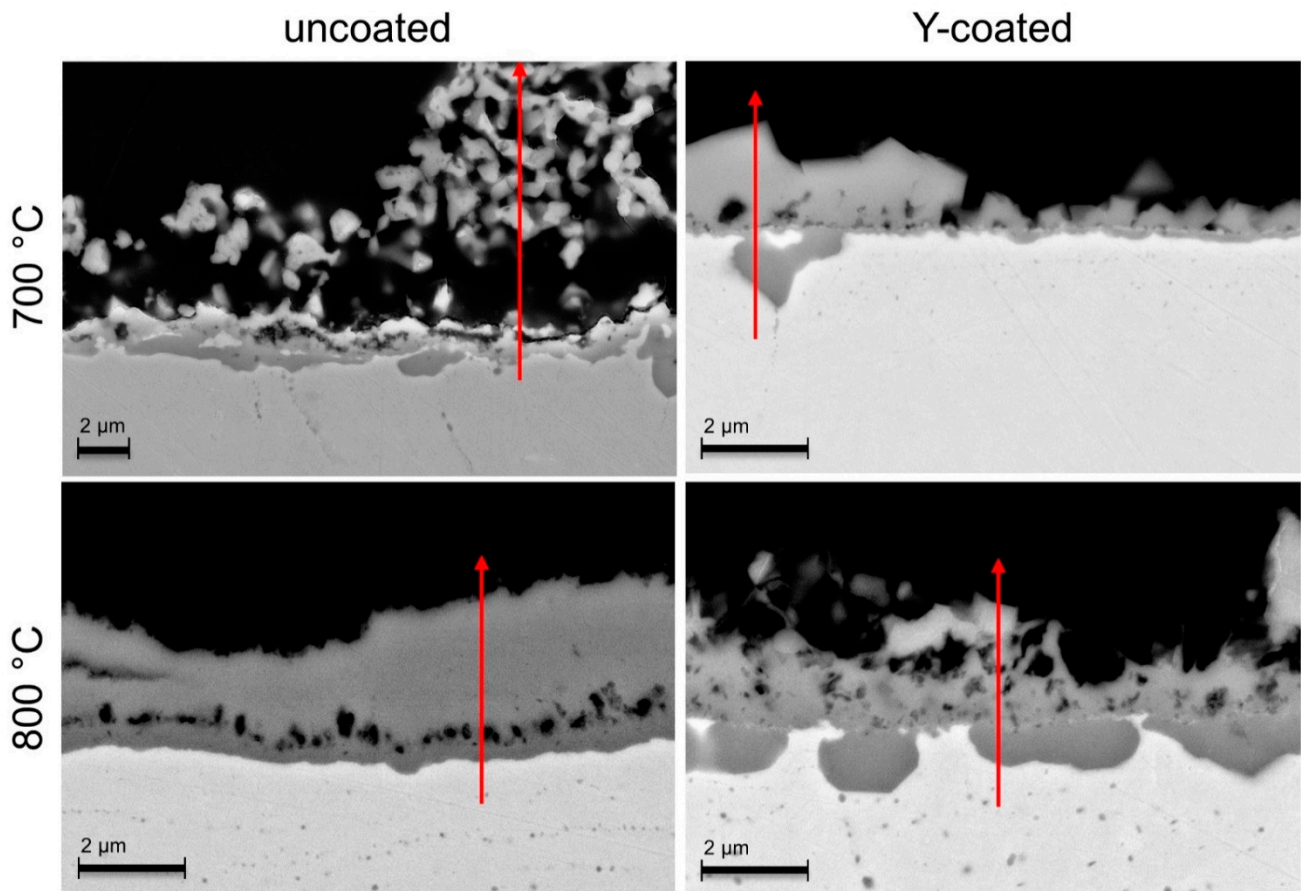
Figure 12. Uncoated Crofer 22 APU (**left**) and Y-coated Crofer 22 APU (**right**) after 1500 h at 700 and 800 °C in reducing atmosphere. The red line indicates the position of the EDS linescan profiles shown in Figure 13.

These differences in scale composition between the samples treated at 700 and 800 °C also produce different morphologies on the samples. The reason for differences in oxide scale structure is the competing inward oxygen and outward cation diffusion processes that are both involved in oxidation behavior of steels. In H_2/H_2O atmosphere, it seems that protective chromia scale formation is promoted at higher temperature, meaning no Fe oxides are found from the sample treated at 800 °C. This is due to the fact that outward Fe diffusion from the steel is quickly blocked by formation of protective chromia scale. As shown by the results in this work, and those reported by Young et al. [11], a temperature difference of 100 °C is sufficiently significant to result in a different behavior.
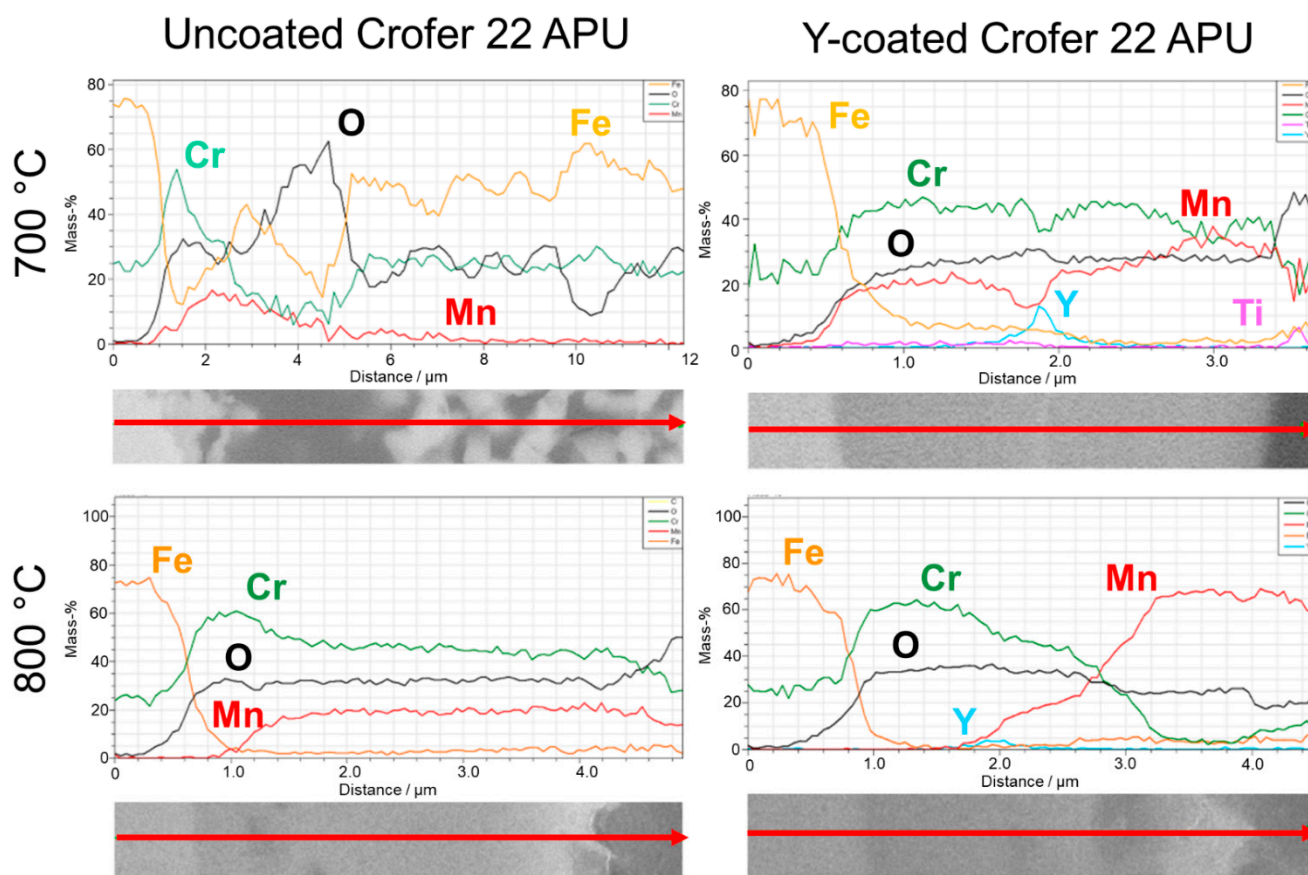
Figure 13. Profile line scans of uncoated Crofer 22 APU (**left**) and Y-coated Crofer 22 APU (**right**) after 1500 h at 700 °C (**top**) and 800 °C (**bottom**) in reducing atmosphere. The red lines in Figure 12 give the places of each.

For the Y-coated Crofer 22 APU exposed for 1500 h at 800 °C, the oxide layer consisted of an inner Cr_2O_3 and an outer $(Mn,Cr)_3O_4$ layer with Y between them (see Figure 13). The morphology of the oxide scale was distinctly different after oxidation at 700 and 800 °C. At 700 °C, the inner scale was in the form of distinct nodules and the outer scale was in the form of facetted crystals. At 800 °C, the nodules of the inner scale were closer to each other, even continuous in some areas, whereas the outer scale was plate/whisker-like.

In AISI 441 (both uncoated and Y-coated) samples, the oxide scale was detached from the steel along most parts of the sample, as can be seen in Figure 14 As no significant scale of spallation was observed after the oxidation of these samples, this detachment likely happened during epoxy mounting. However, the wavy profile of the steel and the smooth profile of the lower part of the oxide layer (at the steel/oxide layer interface) indicates void formation at the steel/oxide scale interface, likely due to cation outward diffusion. Thus, there is a risk of oxide layer spallation with prolonged oxidation. Both the Y-coated and the uncoated AISI 441 formed similar oxide scales consisting of an inner Cr_2O_3 and an outer $(Mn,Cr)_3O_4$ layer (see Figure 15). The Y-coating appears to increase the relative thickness of the inner Cr_2O_3 scale and decrease the overall thickness of the whole oxide scale. The Y-coating did not have any apparent effects on the formation of the SiO_2 scale or the adherence of the oxide scale to the steel substrate.
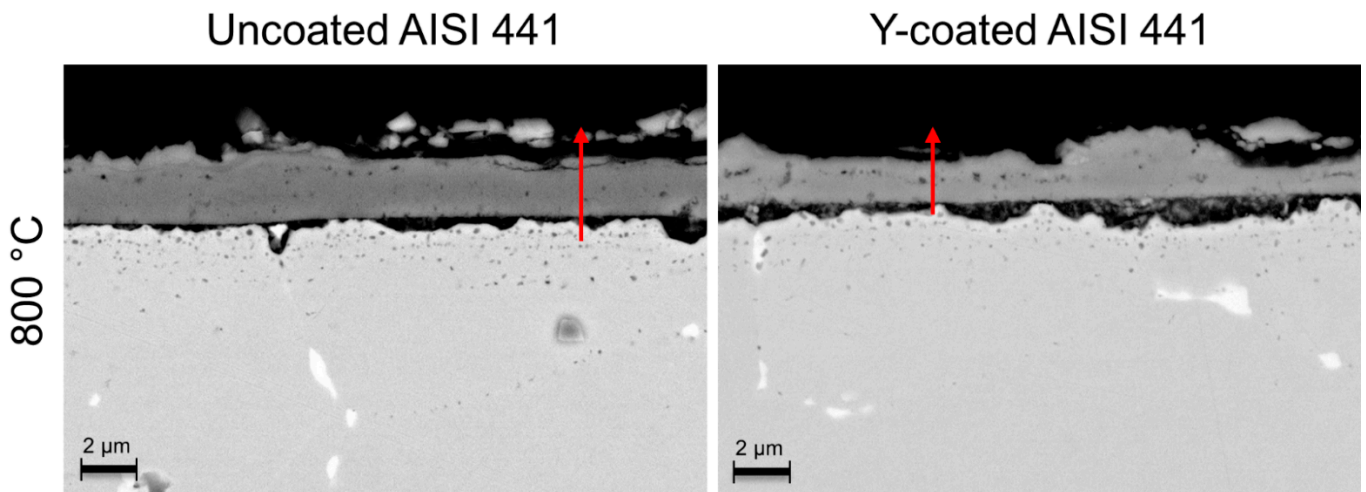
Figure 14. Uncoated AISI 441 (**left**) and Y-coated AISI 441 (**right**) after 1500 h at 800 °C in reducing atmosphere. The red line indicates the place of profiles shown in Figure 15.
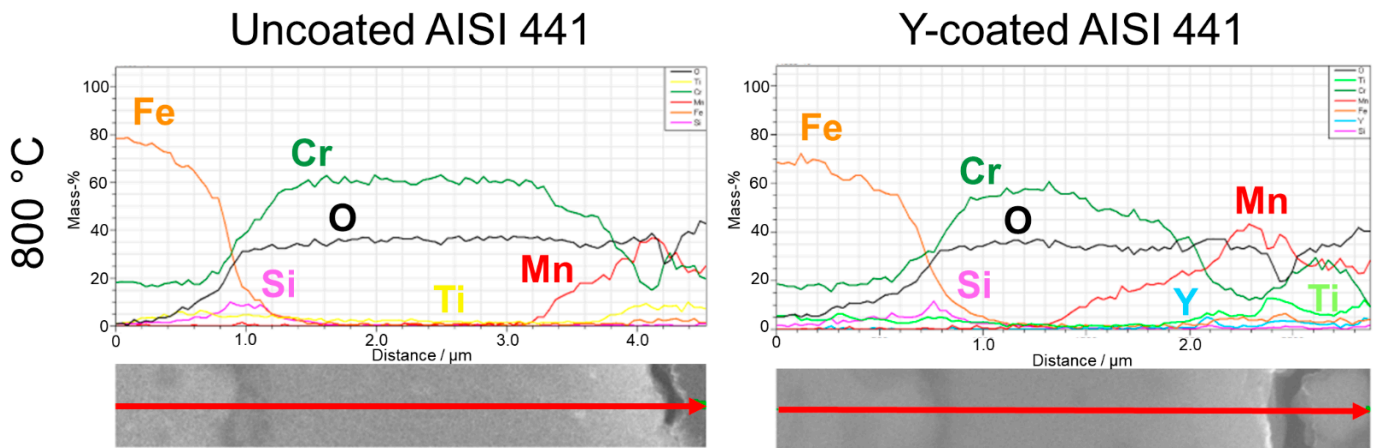

Figure 15. EDS line scans of uncoated AISI 441 (**left**) and Y-coated AISI 441 (**right**) after 1500 h at 800 °C in reducing atmosphere. The red lines (also marked in Figure 14) indicate the location of each profile.

The thicknesses of the oxide scales after oxidation in H_2-H_2O atmosphere are presented in Figure 16. The steel material seems to have little effect on the oxide scale thickness. There is a small decrease in the oxide scale thickness at 800 °C with the Y-coating. More significantly, the Y-coating inhibited the formation of a Fe-oxide layer, thereby decreasing the risk of breakaway corrosion. Thus, the Y-coating is a good candidate for a protective coating for the fuel side on SOEC interconnects.
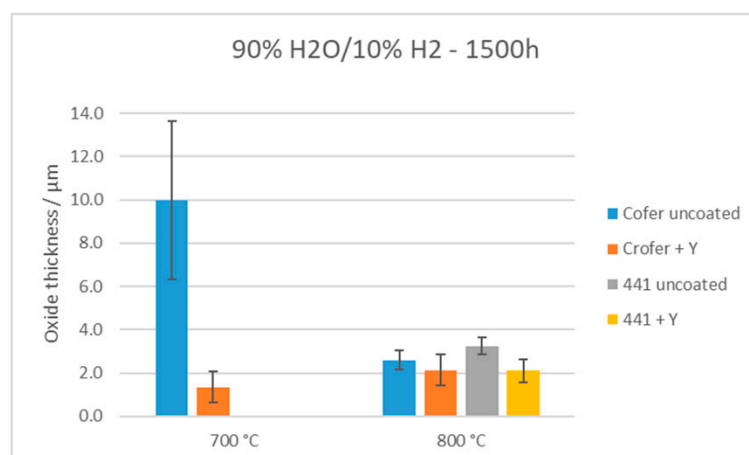
Figure 16. Average oxide scale thicknesses for samples tested in H_2-H_2O atmosphere with standard deviations. For uncoated Crofer 22 APU at 700 °C, the thickness of the porous Fe-oxide layer is included.

4. Conclusions

In this study, protective coatings for both the anodic and cathodic atmospheres present in the SOEC environment were fabricated and tested for 1500 h at 700 and 800 °C on Crofer 22 APU and AISI 441 steels. $Mn_{1.5}Co_{1.5}O_4$ (MCO) spinel produced by electrophoretic deposition, Ce/Co metals deposited by a PVD process, and $LaFeO_3$ (LFO) perovskite applied by a chemical conversion coating process in a molten carbonate bath were evaluated in pure O_2 for the oxygen side. A Y-coating produced by electrolytic deposition was evaluated in 90 vol.% H_2O/10 vol.% H_2 for the hydrogen side. The main obtained results were as follows:

- In pure O_2, the most efficient coatings for limiting the oxide scale formation and Cr outward diffusion were MCO and Ce/Co on Crofer 22 APU at both temperatures. The LFO coating suffered from severe delamination, in particular at 800 °C. With AISI 441, best results were obtained with the MCO coating at both temperatures. Partial delamination of the Ce/Co coating was observed on some of the AISI 441 samples at 800 °C. The oxide scale thickness (Cr_2O_3 and $(Cr,Mn)_3O_4$ layers) was lower with the MCO and Ce/Co coatings compared to the bare steels. Moreover, no or very low Cr content (<5 wt.%) was detected in the MCO and Ce/Co coatings.
- In 90 vol.% H_2O/10 vol.% H_2, the Y-coating tested in this work caused a clear decrease in the oxide scale thickness compared to the bare steels at both temperatures (although AISI 441 was not tested at 700 °C). Additionally, this coating was efficient in avoiding Fe oxide formation, which was observed on the uncoated Crofer 22 APU at 700 °C.
- Globally, the oxide scale adhesion seemed weaker with the AISI 441 steel and voids were observed by SEM at the oxide scale/steel interface in some places of several samples.

In conclusion, the good protective properties of MCO, Ce/Co, and Y-coatings were confirmed in the SOEC environment at the sample level. To complete this study, microstructural characterizations after testing in dual atmospheres and ASR measurements would allow determination of their efficiency in more realistic SOEC conditions and also from an electrical perspective.

Author Contributions: Conceptualization, K.C. and O.T.; methodology, K.C., B.T., B.R.S. and O.T.; formal analysis, J.M., K.C. and B.T.; investigation, K.C., B.T., S.F., N.G., N.P. and O.T.; writing—original draft preparation, J.M.; writing—review and editing, J.M., K.C., B.T., S.F., B.R.S. and O.T.; visualization, J.M. and B.T.; project administration, K.C. and O.T. All authors have read and agreed to the published version of the manuscript.

Conflicts of Interest: The authors declare no conflict of interest.

References

1. Lund, P.D.; Lindgren, J.; Mikkola, J.; Salpakari, J. Review of energy system flexibility measures to enable high levels of variable renewable electricity. *Renew. Sustain. Energy Rev.* **2015**, *45*, 785–807. [CrossRef]
2. Jensen, S.H.; Graves, C.; Mogensen, M.; Wendel, C.; Braun, R.; Hughes, G.; Gao, Z.; Barnett, S.A. Large-scale electricity storage utilizing reversible solid oxide cells combined with underground storage of CO_2 and CH_4. *Energy Environ. Sci.* **2015**, *8*, 2471–2479. [CrossRef]
3. Wang, Y.; Liu, T.; Lei, L.; Chen, F. High temperature solid oxide H_2O/CO_2 co-electrolysis for syngas production. *Fuel Process. Technol.* **2017**, *161*, 248–258. [CrossRef]
4. Buttler, A.; Spliethoff, H. Current status of water electrolysis for energy storage, grid balancing and sector coupling via power-to-gas and power-to-liquids: A review. *Renew. Sustain. Energy Rev.* **2018**, *82*, 2440–2454. [CrossRef]
5. Mahato, N.; Banerjee, A.; Gupta, A.; Omar, S.; Balani, K. Progress in material selection for solid oxide fuel cell technology: A review. *Prog. Mater. Sci.* **2015**, *72*, 141–337. [CrossRef]
6. Sun, C.; Hui, R.; Roller, J. Cathode materials for solid oxide fuel cells: A review. *J. Solid State Electrochem.* **2010**, *14*, 1125–1144. [CrossRef]
7. Singhal, S.; Kendall, K.; Kendall, M. *High-Temperature Solid Oxide Fuel Cells: Fundamentals, Design and Applications*; Elsevier: Amsterdam, The Netherlands, 2015. [CrossRef]
8. Wu, J.; Liu, X. Recent development of SOFC metallic interconnect. *J. Mater. Sci. Technol.* **2010**, *26*, 293–305. [CrossRef]
9. Palcut, M.; Mikkelsen, L.; Neufeld, K.; Chen, M.; Knibbe, R.; Hendriksen, P.V. Corrosion stability of ferritic stainless steels for solid oxide electrolyser cell interconnects. *Corros. Sci.* **2010**, *52*, 3309–3320. [CrossRef]
10. Alnegren, P.; Sattari, M.; Froitzheim, J.; Svensson, J.E. Degradation of ferritic stainless steels under conditions used for solid oxide fuel cells and electrolyzers at varying oxygen pressures. *Corros. Sci.* **2016**, *110*, 200–212. [CrossRef]
11. Young, D.J.; Zurek, J.; Singheiser, L.; Quadakkers, W.J. Temperature dependence of oxide scale formation on high-Cr ferritic steels in $Ar-H_2-H_2O$. *Corros. Sci.* **2011**, *53*, 2131–2141. [CrossRef]
12. Shaigan, N.; Qu, W.; Ivey, D.G.; Chen, W. A review of recent progress in coatings, surface modifications and alloy developments for solid oxide fuel cell ferritic stainless steel interconnects. *J. Power Sources* **2010**, *195*, 1529–1542. [CrossRef]
13. Mah, J.C.W.; Muchtar, A.; Somalu, M.R.; Ghazali, M.J. Metallic interconnects for solid oxide fuel cell: A review on protective coating and deposition techniques. *Int. J. Hydrogen Energy* **2017**, *42*, 9219–9229. [CrossRef]
14. Yang, Z.; Xia, G.G.; Maupin, G.D.; Stevenson, J.W. Conductive protection layers on oxidation resistant alloys for SOFC interconnect applications. *Surf. Coat. Technol.* **2006**, *201*, 4476–4483. [CrossRef]
15. Froitzheim, J.; Canovic, S.; Nikumaa, M.; Sachitanand, R.; Johansson, L.G.; Svensson, J.E. Long term study of Cr evaporation and high temperature corrosion behaviour of Co coated ferritic steel for solid oxide fuel cell interconnects. *J. Power Sources* **2012**, *220*, 217–227. [CrossRef]
16. Lacey, R.; Pramanick, A.; Lee, J.C.; Jung, J.-I.; Jiang, B.; Edwards, D.D.; Naum, R.; Misture, S.T. Evaluation of Co and perovskite Cr-blocking thin films on SOFC interconnects. *Solid State Ion.* **2010**, *181*, 1294–1302. [CrossRef]
17. Mardare, C.C.; Asteman, H.; Spiegel, M.; Savan, A.; Ludwig, A. Investigation of thermally oxidised Mn-Co thin films for application in SOFC metallic interconnects. *Appl. Surf. Sci.* **2008**, *255*, 1850–1859. [CrossRef]
18. Uehara, T.; Yasuda, N.; Okamoto, M.; Baba, Y. Effect of Mn-Co spinel coating for Fe-Cr ferritic alloys ZMG232L and 232J3 for solid oxide fuel cell interconnects on oxidation behavior and Cr-evaporation. *J. Power Sources* **2011**, *196*, 7251–7256. [CrossRef]
19. Ajitdoss, L.C.; Smeacetto, F.; Bindi, M.; Beretta, D.; Salvo, M.; Ferraris, M. $Mn_{1.5}Co_{1.5}O_4$ protective coating on Crofer22APU produced by thermal co-evaporation for SOFCs. *Mater. Lett.* **2013**, *95*, 82–85. [CrossRef]
20. Gavrilov, N.V.; Ivanov, V.V.; Kamenetskikh, A.S.; Nikonov, A.V. Investigations of Mn-Co-O and Mn-Co-Y-O coatings deposited by the magnetron sputtering on ferritic stainless steels. *Surf. Coat. Technol.* **2011**, *206*, 1252–1258. [CrossRef]
21. Balland, A.; Gannon, P.; Deibert, M.; Chevalier, S.; Caboche, G.; Fontana, S. Investigation of La_2O_3 and/or $(Co,Mn)_3O_4$ deposits on Crofer22APU for the SOFC interconnect application. *Surf. Coat. Technol.* **2009**, *203*, 3291–3296. [CrossRef]
22. Yang, Z.; Xia, G.; Nie, Z.; Templeton, J.; Stevenson, J.W. Ce-modified $(Mn,Co)_3O_4$ spinel coatings on ferritic stainless steels for SOFC interconnect applications. *Electrochem. Solid-State Lett.* **2008**, *11*, B140–B143. [CrossRef]
23. Hoyt, K.O.; Gannon, P.E.; White, P.; Tortop, R.; Ellingwood, B.J.; Khoshuei, H. Oxidation behavior of $(Co,Mn)_3O_4$ coatings on preoxidized stainless steel for solid oxide fuel cell interconnects. *Int. J. Hydrogen Energy* **2012**, *37*, 518–529. [CrossRef]
24. Tallgren, J.; Bianco, M.; Mikkola, J.; Himanen, O.; Kiviaho, J.; van Herle, J. Comparison of different manganese-cobalt-iron spinel protective coatings for SOFC interconnects. In Proceedings of the 12th European SOFC & SOE Forum, Lucerne, Switzerland, 5–8 July 2016; p. B0619.

25. Tallgren, J.; Bianco, M.; Himanen, O.; Thomann, O.; Kiviaho, J.; van Herle, J. Evaluation of protective coatings for SOFC interconnects. *ECS Trans.* **2015**, *68*, 1597–1608. [CrossRef]

26. Kruk, A.; Stygar, M.; Brylewski, T. Mn-Co spinel protective-conductive coating on AL453 ferritic stainless steel for IT-SOFC interconnect applications. *J. Solid State Electrochem.* **2013**, *17*, 993–1003. [CrossRef]

27. Thomann, O.; Pihlatie, M.; Rautanen, M.; Himanen, O.; Lagerbom, J.; Mäkinen, M.; Varis, T.; Suhonen, T.; Kiviaho, J. Development and application of HVOF sprayed spinel protective coating for SOFC interconnects. *J. Therm. Spray Technol.* **2013**, *22*, 631–639. [CrossRef]

28. Talic, B.; Molin, S.; Wiik, K.; Hendriksen, P.V.; Lein, H.L. Comparison of iron and copper doped manganese cobalt spinel oxides as protective coatings for solid oxide fuel cell interconnects. *J. Power Sources* **2017**, *372*, 145–156. [CrossRef]

29. Talic, B.; Falk-Windisch, H.; Venkatachalam, V.; Hendriksen, P.V.; Wiik, K.; Lein, H.L. Effect of coating density on oxidation resistance and Cr vaporization from solid oxide fuel cell interconnects. *J. Power Sources* **2017**, *354*, 57–67. [CrossRef]

30. Falk-Windisch, H.; Claquesin, J.; Sattari, M.; Svensson, J.E.; Froitzheim, J. Co- and Ce/Co-coated ferritic stainless steel as interconnect material for intermediate temperature solid oxide fuel cells. *J. Power Sources* **2017**, *343*, 1–10. [CrossRef]

31. Falk-Windisch, H.; Sattari, M.; Svensson, J.E.; Froitzheim, J. Chromium vaporization from mechanically deformed pre-coated interconnects in solid oxide fuel cells. *J. Power Sources* **2015**, *297*, 217–223. [CrossRef]

32. Falk-Windisch, H.; Svensson, J.E.; Froitzheim, J. The effect of temperature on chromium vaporization and oxide scale growth on interconnect steels for solid oxide fuel cells. *J. Power Sources* **2015**, *287*, 25–35. [CrossRef]

33. Grolig, J.G.; Froitzheim, J.; Svensson, J.-E. Effect of cerium on the electrical properties of a cobalt conversion coating for solid oxide fuel cell interconnects—A study using impedance spectroscopy. *Electrochim. Acta* **2015**, *184*, 301–307. [CrossRef]

34. Grolig, J.G.; Froitzheim, J.; Svensson, J.E. Coated stainless steel 441 as interconnect material for solid oxide fuel cells: Oxidation performance and chromium evaporation. *J. Power Sources* **2014**, *248*, 1007–1013. [CrossRef]

35. Berger, R.; Lundberg, M.W.; Westlinder, J. Self-healing of precoated AISI 441 for solid oxide fuel cell interconnects at intermediate temperatures. *ECS Trans.* **2017**, *78*, 1599–1605. [CrossRef]

36. Molin, S.; Chen, M.; Hendriksen, P.V. Oxidation study of coated Crofer 22 APU steel in dry oxygen. *J. Power Sources* **2014**, *251*, 488–495. [CrossRef]

37. Frangini, S.; della Seta, L.; Masi, A.; Paoletti, C.; Bianco, M. Perovskite conversion coatings as novel and simple approach for improving functional performance of ferritic stainless steel SOFC interconnects. *Fuel Cells* **2020**, *20*, 316–322. [CrossRef]

38. Frangini, S.; della Seta, L.; Paoletti, C. Effect of additive particle size on the CuO-accelerated formation of $LaFeO_3$ perovskite conversion coatings in molten carbonate baths. *Surf. Coat. Technol.* **2019**, *374*, 513–520. [CrossRef]

39. Frangini, S.; Masi, A.; della Seta, L.; Bianco, M.; van Herle, J. Composite Cu-$LaFeO_3$ conversion coatings on a 18Cr ferritic stainless steel for IT-SOFC interconnects: Effect of long-term air exposure at 700 °C on Cr diffusion barrier and electrical properties. *J. Electrochem. Soc.* **2018**, *165*, F97–F104. [CrossRef]

40. Sachitanand, R.; Sattari, M.; Svensson, J.E.; Froitzheim, J. The oxidation of coated SOFC interconnects in fuel side environments. *Fuel Cells* **2016**, *16*, 32–38. [CrossRef]

41. Ardigo, M.R.; Popa, I.; Combemale, L.; Chevalier, S.; Herbst, F.; Girardon, P. Dual atmosphere study of the K41X stainless steel for interconnect application in high temperature water vapour electrolysis. *Int. J. Hydrogen Energy* **2014**, *40*, 5305–5312. [CrossRef]

42. Nakamura, T.; Petzow, G.; Gauckler, L.J. Stability of the perovskite phase $LaBO_3$ (B = V, Cr, Mn, Fe, Co, Ni) in reducing atmosphere I. Experimental results. *Mater. Res. Bull.* **1979**, *14*, 649–659. [CrossRef]

43. Molin, S.; Persson, Å.H.; Skafte, T.; Smitshuysen, A.; Jensen, S.; Andersen, K.; Xu, H.; Chen, M.; Hendriksen, P. Effective yttrium based coating for steel interconnects of solid oxide cells: Corrosion evaluation in steam-hydrogen atmosphere. *J. Power Sources* **2019**, *440*, 226814. [CrossRef]

44. VDM Metals. VDM®Crofer 22 APU. 2010. Available online: www.vdm-metals.com/fileadmin/user_upload/Downloads/Data_Sheets/Datenblatt_VDM_Crofer_22_APU.pdf (accessed on 10 February 2020).

45. Thyssenkrupp. Thyssenkrupp Stainless Steel 441 1.4509. 2001. Available online: www.thyssenkrupp-materials.co.uk/media/material_data_sheets/stainless_steel_1/stainless_steel_1-4509_441.pdf (accessed on 10 February 2020).

46. Bobruk, M.; Molin, S.; Chen, M.; Brylewski, T.; Hendriksen, P.V. Sintering of $MnCo_2O_4$ coatings prepared by electrophoretic deposition. *Mater. Lett.* **2018**, *213*, 394–398. [CrossRef]

47. Canovic, S.; Froitzheim, J.; Sachitanand, R.; Nikumaa, M.; Halvarsson, M.; Johansson, L.-G.; Svensson, J.-E. Oxidation of Co- and Ce-nanocoated FeCr steels: A microstructural investigation. *Surf. Coat. Technol.* **2013**, *215*, 62–74. [CrossRef]

48. Chen, Z.; Wang, L.; Li, F.; Chou, K.C.; Sun, Z. The effects of temperature and oxygen pressure on the initial oxidation of stainless steel 441. *Int. J. Hydrogen Energy* **2014**, *39*, 10303–10312. [CrossRef]

49. Lorenzo, M.D.J.; Kolarik, V.; Kuchenreuther-Hummel, V.; Pötschke, M.; Schimanke, D. Oxidation of La–Sr–Mn-coated interconnector alloys for steam electrolysis under pressure in pure oxygen and in pure steam. *Oxid. Met.* **2017**, *88*, 279–290. [CrossRef]

50. Yang, Z.; Xia, G.; Wang, C.M.; Nie, Z.; Templeton, J.D.; Singh, P.; Stevenson, J.W. *Investigation of AISI 441 Ferritic Stainless Steel and Development of Spinel Coatings for SOFC Interconnect Applications*; U.S. Department of Energy: Washington, DC, USA, 2008.

51. Chandra-Ambhorn, S.; Wouters, Y.; Antoni, L.; Toscan, F.; Galerie, A. Adhesion of oxide scales grown on ferritic stainless steels in solid oxide fuel cells temperature and atmosphere conditions. *J. Power Sources* **2007**, *171*, 688–695. [CrossRef]
52. Mougin, J.; Dupeux, M.; Antoni, L.; Galerie, A.A. Adhesion of thermal oxide scales grown on ferritic stainless steels measured using the inverted blister test. *Mater. Sci. Eng. A* **2003**, *359*, 44–51. [CrossRef]
53. Ebrahimifar, H.; Zandrahimi, M. Evaluation of the parabolic rate constant during different types of oxidation tests for spinel coated Fe-17%Cr alloy. *Oxid. Met.* **2011**, *75*, 125–141. [CrossRef]